Measurements of ionization states in warm dense aluminum with betatron radiation

M. Z. Mo,[1,*] Z. Chen,[1,†] S. Fourmaux,[2] A. Saraf,[2] S. Kerr,[1] K. Otani,[2] R. Masoud,[1] J.-C. Kieffer,[2] Y. Tsui,[1] A. Ng,[3] and R. Fedosejevs[1,‡]

[1]*Department of Electrical and Computer Engineering, University of Alberta, Edmonton, Alberta, Canada, T6G 2V4*

[2]*INRS-EMT, Université du Québec, 1650 Lionel Boulet, Varennes, Quebéc, Canada, J3X 1S2*

[3]*Department of Physics and Astronomy, University of British Columbia, Vancouver, British Columbia, Canada, V6T 1Z1*

(Received 18 February 2017; published 19 May 2017)

Time-resolved measurements of the ionization states of warm dense aluminum via K-shell absorption spectroscopy are demonstrated using betatron radiation generated from laser wakefield acceleration as a probe. The warm dense aluminum is generated by irradiating a free-standing nanofoil with a femtosecond optical laser pulse and was heated to an electron temperature of ∼20–25 eV at a close-to-solid mass density. Absorption dips in the transmitted x-ray spectrum due to the Al^{4+} and Al^{5+} ions are clearly seen during the experiments. The measured absorption spectra are compared to simulations with various ionization potential depression models, including the commonly used Stewart-Pyatt model and an alternative modified Ecker-Kröll model. The observed absorption spectra are in approximate agreement with these models, though indicating a slightly higher state of ionization and closer agreement for simulations with the modified Ecker-Kröll model.

DOI: 10.1103/PhysRevE.95.053208

I. INTRODUCTION

Warm dense matter (WDM) with a temperature typically in the range of 1–50 eV and density 0.1–10 times the solid density commonly exists in the cores of giant planets [1,2]. With the advent of ultrafast (<1 ps) energy sources, such as optical lasers [3], free electron lasers [4,5], and protons [6], WDM can also be generated by isochorically heating solids. Since the energy is mostly deposited into the electron system, the resultant WDM usually has a much higher electron temperature (T_e) than the ions (T_i) for a few to a few tens of picoseconds as the electrons couple energy to the ions [7,8]. New challenges exist in understanding nonequilibrium WDM in such quickly evolving systems, since the knowledge of WDM in equilibrium may not be fully valid under such conditions. One important parameter in understanding WDM is the ionization state, which affects the thermal and transport properties.

A key factor affecting the ionization state in dense plasma is ionization potential depression (IPD), in which the surrounding ambient plasma gives rise to an ionization potential lower than that of an isolated ion. A number of analytical models have been developed to calculate the IPD [9–12]. However, there are few rigorous experimental benchmarks to validate such models due to the great challenge in measuring the IPD accurately. This challenge was recently addressed by taking advantage of ultraintense x-ray free-electron lasers [4,5]. In those studies, the measured IPDs inferred from the edge shifts of the K_α emission spectra from x-ray-heated ($70 < T_e < 180$ eV) solid-density aluminum were found to be in best agreement with the Ecker and Kröll (EK) IPD model [9], compared to the Stewart-Pyatt (SP) [10] and ion-sphere (IS) models [11,12]. Another recent study on hot dense aluminum plasma ($500 < T_e < 700$ eV, $1 < \rho < 10$ g/cm^3), however, found that the measured density dependence of the Ly_β emission lines was in closer agreement with simulations using the SP model of IPD rather than those using the EK model [13]. More recently, a study on highly compressed WDM (CH shell, $5 < T_e < 10$ eV, $2 < \rho < 9$ g/cm^3) with x-ray Thomson scattering observed the IPD effect and demonstrated the significance of including the IPD effect in radiation-hydrodynamic simulations [14]. Nonetheless, no significant differences in the simulations using the EK and SP models were seen under their experimental conditions. Based on the studies reported to date, it appears that the validity of the EK and SP models is sensitive to the plasma regime. Hence further experimental studies are necessary to map out the full-scale validity of various IPD models over different plasma regimes.

It is in this context that we report a study of ionization states of warm dense aluminum heated by a femtosecond laser pulse [15]. The experimental data presented in our study differ from those in previous studies in that a tabletop ultrafast x-ray probe, broad-band betatron radiation [16–19] generated from laser wakefield acceleration (LWFA), was employed for the first time to diagnose the ionization dynamics through K-shell line absorption spectroscopy. Each ionization state is identified by its distinct K-L bound-bound absorption line, which shifts in energy as the electron screening is reduced with increasing ionization. Under our experimental conditions of $T_e \sim 20$–25 eV and $\rho \sim 2.7$ g/cm^3, ionization stages of Al^{3+} to Al^{6+} are expected with vacuum ionization potentials of 28.4, 120.0, 153.8, and 190.5 eV to create these levels, respectively [20]. At solid density and for a temperature of 20 eV the expected IPD for the Al^{4+} is of the order of 47 eV for the SP model to 74 eV for the modified Ecker and Kröll (mEK) model [21,22]. Thus the magnitude of the IPD expected is a significant fraction of the ionization potential of 153.8 eV from the Al^{4+} to the Al^{5+} state. Thus differing ionization distributions can be expected for the different models. In our measurements we find that the measured time-dependent absorption spectra are in closer agreement with calculations using the EK model than those using SP and IS models, in line with what was found in Ref. [5].

*mmo@ualberta.ca; Present address: SLAC National Accelerator Laboratory, Menlo Park, California 94025, USA.

†Present address: SLAC National Accelerator Laboratory, Menlo Park, California 94025, USA.

‡rfed@ualberta.ca

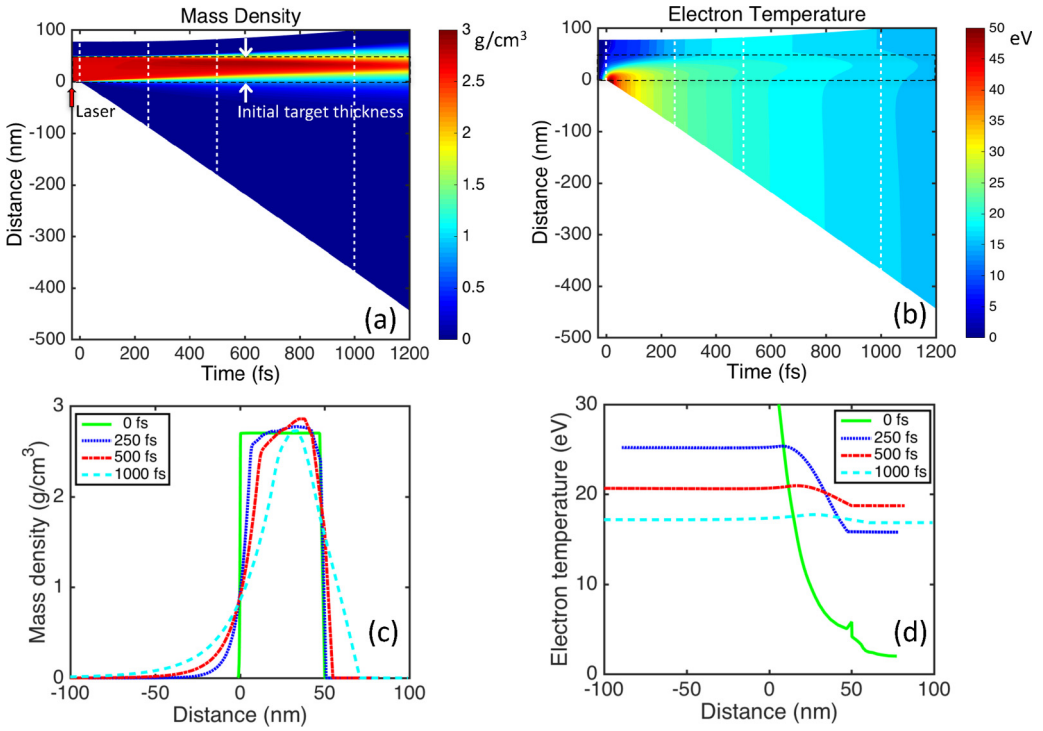

FIG. 1. (a, b) Contour plots of the MULTI-FS simulated mass density $\rho(r,t)$ and electron temperature $T_e(r,t)$ of a 50-nm Al foil as a function of the axial position and time, irradiated with a 30-fs laser pulse at an absorbed intensity of 4.6×10^{14} W/cm^2 in the laser propagation direction and a wavelength of 800 nm. The laser impinges on the target from the bottom with an angle of incidence of 40° and p polarization. Zero time was defined as the time when the peak of the laser reached the target. (c, d) Spatial line-outs of the mass density and plasma temperature, respectively, for four times as indicated by the dashed white lines overlain on the contour plots. In the simulation, an artificial layer of aluminum vapor (2×10^{-4} g/cm^3) was added at the back of the target to observe the rear expansion. This artificial layer is so dilute that its effect on the mass expansion and heat propagation in the rear side is negligible.

II. EXPERIMENTAL DETAILS

The pump-probe experiment was performed at the Advanced Laser Light Source facility located at INRS, Varennes [23,24]. The configuration of the betatron probe has been described in detail elsewhere [19]. The betatron radiation from laser wakefield acceleration was obtained by focusing an 800-nm laser pulse with a pulse duration of 30 fs (FWHM) and pulse energy of 2.4 J onto a supersonic helium gas jet target. The betatron radiation had a photon flux of the order of 10^8 photons/srad/0.1%BW/shot at 1.5 keV and a divergence of the order of 20 mrad (FWHM). The x-ray pulse was focused with an adjustable Kirkpatrick-Baez microscope onto the target to be studied with an incident angle of 38.5° and the x-ray spot at the target position was approximately 50 μm (FWHM). The target studied in the experiment was 50 nm free-standing aluminum foil that was mounted over an aperture 500 μm in diameter. Targets were prepared by sputter deposition and thicknesses measured using a stylus profiler with 2% accuracy. The density of such targets is expected to be within 3%–7% of the bulk density [25].

The spectrum of the transmitted x rays was resolved by a flat potassium acid phthalate (KAP) Bragg crystal spectrometer. The KAP Bragg crystal has a 2d spacing of 26.63 Å and the first diffraction order was used to measure the x-ray energies around 1.5 keV. The x-ray CCD (Princeton Instruments; PI MTE, 1300B) used for the spectrometer was a vacuum-compatible back-illuminated CCD without AR coating. The entire betatron probe system had a spectral resolution of 1.5 eV, a detection bandwidth of 24 eV, and an overall photon throughput efficiency of the order of 10^{-5} [19]. The photon energy scale was calibrated by observing the absorption k-edge of cold aluminum and then rotating the crystal by a fixed angular offset, yielding a final photon energy accuracy of ∼2 eV. Within the spectrally resolved detection band, approximately 10 photons were detected by the x-ray CCD per laser shot. Thus, in the experiment, hundreds of shots were acquired per absorption spectrum to observe the K-shell absorption features expected from the ionization states of the warm dense aluminum.

The synchronized pump laser or heater pulse for creating the warm dense aluminum was picked off from the edge of the main laser pulse driving the plasma wakefields and its path length was adjusted by a motorized delay stage installed in the LWFA chamber. The heater pulse was p-polarized and imaged onto the aluminum target at an incident angle of 40° in a spot approximately 200 μm in diameter. In this experiment, the pulse energy of the heater at the target was fixed at 10 mJ, giving an average intensity of $1.1 \pm 0.2 \times 10^{15}$ W/cm^2 in the laser propagation direction in the 50-μm spot probed by the betatron radiation using the experimentally measured heater beam intensity profile. The energy of the reflection of the heater pulse after interacting with the Al target was measured with a calibrated photodiode detector. The absorption coefficient of the heater pulse under the experimental conditions was measured as approximately $41\% \pm 6\%$, giving an average

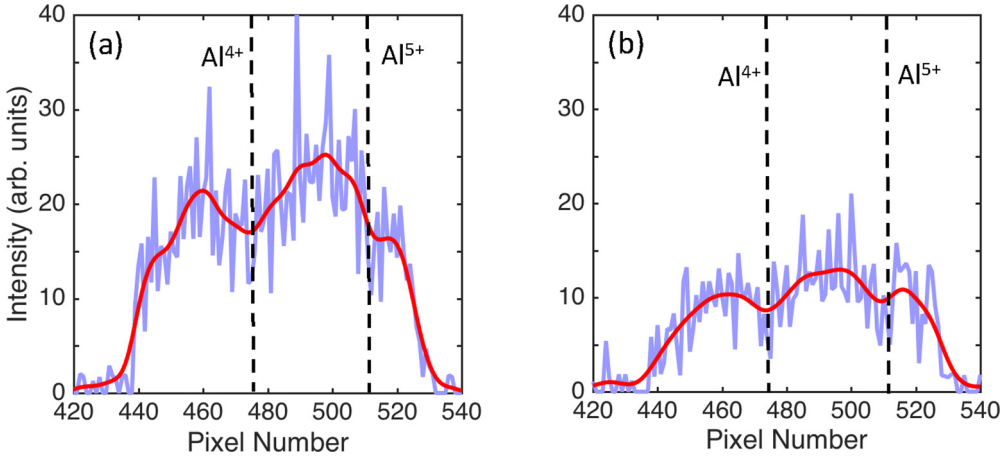

FIG. 2. (a) Raw x-ray spectrum (light-blue line) measured at $t = 0.5$ ps and a Gaussian smoothed fit to the curve (red line). The FWHM of the Gaussian function for smoothing this measured spectrum was 7 pixels, corresponding to a spectral width of 2.1 eV. (b) The same as (a), but for $t = 1$ ps. The FWHM of the Gaussian smoothing function was 9 pixels (2.7 eV). The positions of the observed Al^{4+} and Al^{5+} absorption dips at these two delays are shown by the dashed vertical lines.

absorbed intensity of $4.5 \pm 0.7 \times 10^{14}$ W/cm^2 in the laser propagation direction.

The one-dimensional hydrodynamic code MULTI-FS [26] was employed to model the hydrodynamic expansion of the target. This code correctly accounts for resonance absorption on the femtosecond time scale using an electromagnetic wave solver [27]. The plasma model that accounts for the electron-ion collision frequency was based on the Drude-Sommerfeld theory [28]. The resultant lag in heating of the ions leads to an ion temperature of only a few electron volts during the first picosecond. In MULTI-FS, the equation of state of the matter to be studied is interpolated from tables generated from the MPQEOS code [29], whereas the opacities and ionization are interpolated from tables generated from the SNOP atomic physics code [30]. Ionization potential depression is taken into account by the SNOP code and is based on More's ion-sphere model [11,12].

III. RESULTS

Figures 1(a) and 1(b) illustrate, respectively, the time evolution of the mass density and electron temperature for 50 nm Al irradiated under the same laser conditions as the experiment. The calculation was carried out for an absorbed intensity of 4.6×10^{14} W/cm^2. It is shown that the front target expansion (on the laser side) starts a few tens of femtoseconds after the laser peak reaches the target, as opposed to the rear target expansion, which occurs approximately 0.5 ps later. The heating of the target is fairly nonuniform for the first 100 fs but after 500 fs the heating becomes uniform.

The raw x-ray transmission spectra measured at 0.5 and 1 ps after the Al target was heated are shown in Fig. 2 together with their corresponding smoothed spectra. For convenience, we define the spectrum achieved with pump and probe together as the full-shot spectrum and the one without the pump as the reference spectrum. The total numbers of full and reference shots acquired for these two spectra are 174 and 150, respectively. Due to the finite number of x-ray photons arriving at the detector the raw signal is quite noisy. However, after smoothing the raw spectra with a Gaussian smoothing function, the absorption dips by ions Al^{4+} and Al^{5+}, as labeled in Fig. 2, become apparent. The reference shots with unheated targets in place were interleaved with the full data shots so that any systematic drifts in the experiment were taken into account.

The measured transmission of the x rays is obtained by dividing the smoothed full-shot spectrum by its reference spectrum. The resultant x-ray transmission curves are plotted in Fig. 3 by the dashed green lines. The measured x-ray transmission curves have been normalized to minimize the discrepancy in the baseline transmission between the measurement and the average of three model calculations (discussed below) at the wavelengths of 1484 and 1494 eV, where little absorption is expected. This is done to correct for variations in the absolute x-ray fluence during the series of measurements. While there is some experimental uncertainty in this average transmission factor, it does not affect the overall shapes of the measured transmission spectra. While the betatron fluence varies significantly from shot to shot, the betatron spectrum is very smooth over the small, 25-eV window and does not contribute to any spectral features in this window. The error bar of the measurement, shown as the shaded area in Fig. 3, was defined as $\sigma_i = \sqrt{1/n_i + 1/m_i}$, where n_i and m_i are the number of photons in bin i within a smoothing bandwidth of the full-shot spectrum and its reference, respectively. For the measured spectra as shown in Fig. 2, this smoothing bandwidth was set to 3 eV to account for the smoothing function (2.1–2.7 eV), instrumental resolution (1.4 eV), and expected line widths (1.2–1.5 eV).

As shown in Fig. 3, the observed K_α absorption lines ($1s-2p$) of the Al^{4+} and Al^{5+} ions are located at ~1.49 and ~1.50 keV, respectively. The shift in the line position of Al^{5+} from Al^{4+} is due to the weaker screening effect of the nuclear charge from the lesser number of bound electrons. Another feature that can be clearly observed is the decrease in the depth of the absorption dip with time for each ion species, implying that some portion of the ions has recombined with the free electrons during this time period.

To further interpret the measured K_α absorption spectra and to understand the underlying ionization dynamics of the warm

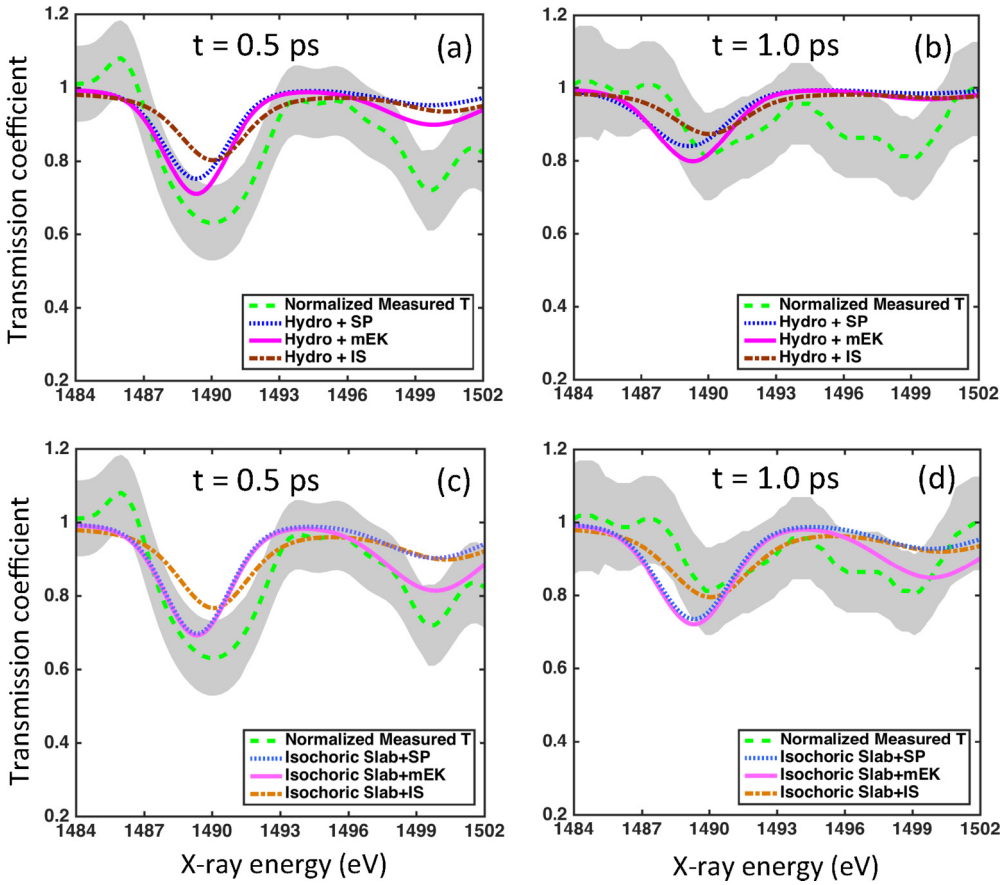

FIG. 3. Comparison of the measured transmission curves (dashed green curves) at delays of 0.5 and 1 ps with the simulated transmission curves obtained with different models. The measured transmission curve was normalized to compare with the simulations. The gray area represents the error bar of the measured transmission. (a, b) Simulation results were obtained based on MULTI-FS hydro simulations and spectroscopic calculations with the Stewart-Pyatt (SP), modified Ecker and Kröll (mEK), and ion-sphere (IS) IPD models. (c, d) Simulation results were obtained based on a MULTI-FS simulation with hydro expansion turned off to suppress expansion cooling, using spectroscopic calculations similar to those used in (a) and (b).

dense aluminum, it is necessary to compare with simulations. To do that, two atomic physics codes, PRISMSPECT [31] and FLYCHK [32], were employed. Both codes follow the collisional-radiative population kinetics approach in which the detailed configuration accounting (DCA) or superconfiguration [33] atomic model was included. IPD is taken into account in both physics codes, but with different models. In PRISMSPECT, the model employed is based on the IS average atom model [11,12], whereas in FLYCHK, the SP [10] and mEK [21] models are provided.

The initial plasma conditions, i.e., the mass density and electron temperature, for spectroscopic simulation were taken directly from the MULTI-FS simulation at the two time delays of our measurements, as shown in Figs. 1(c) and 1(d). Steady-state calculations of absorption were performed to study our cases of interest. Thermal equilibrium ($T_e = T_i$) was assumed in these calculations. The calculated opacities $\kappa(\nu)_i$ for cell i of the MULTI-FS simulated target from the two atomic codes were extracted and substituted into the equation $T(\nu) = \exp(-\sum_{i=1}^{n} \kappa(\nu)_i \rho_i R_i / \cos(\theta))$ to compute the total transmission $T(\nu)$, where n is the total number of cells in the MULTI-FS simulation, ρ_i and R_i are the mass density and thickness of cell i, respectively, and θ is the betatron incident angle. The calculated transmission was then convolved with a Gaussian function with an FWHM equal to the combined instrumental and smoothing resolutions used for the experimental data.

IV. DISCUSSION

The simulated transmission curves obtained with the above-mentioned algorithm are illustrated in Figs. 3(a) and 3(b) to compare with the measurements. For FLYCHK simulations, runs with both the SP and the mEK models of IPD are implemented for comparison. The expected line positions for Al^{4+} and Al^{5+} ions from the two codes both indicate a good agreement with the measured positions within the spectral measurement error bar of ± 2 eV. Regarding the time-dependent line absorption depth, qualitatively, the simulations with both codes are in reasonable agreement with the measurement of Al^{4+} absorption near 1490 eV regardless of the IPD models employed.

Discrepancies in the transmission coefficient at the Al^{5+} position between the simulations and measurements are clearly shown in Figs. 3(a) and 3(b). The discrepancies could be due in part to the fact that the different temperatures between the electrons and ions and the residual lattice structure in the ion

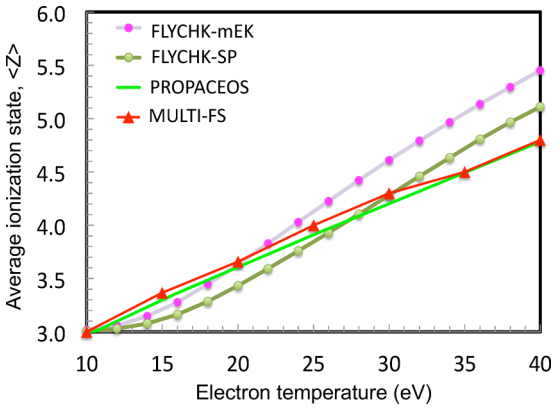

FIG. 4. Comparison of the $\langle Z \rangle$ of Al at solid density as a function of the temperature derived from different ionization models.

component are not accounted for by the two atomic physics codes. More sophisticated simulations such as first-principle calculations based on density functional theory [34] may be necessary to understand these discrepancies, which is beyond the scope of the current investigation. However, given the relatively large error bar on the absorbed energy, part of the difference could be explained if the absorbed energy were higher than measured.

Differences in the ionization state used in the MULTI-FS hydrocode and the atomic physics codes could also lead to some discrepancy in the results. Figure 4 depicts the temperature dependence of the average ionization state $\langle Z \rangle$ of solid-density Al derived from MULTI-FS, FLYCHK with IPD models mEK and SP, and the PROPACEOS model [35] used by PRISMSPECT. As shown, within the displayed temperature window, similar trends of $\langle Z \rangle$ are observed. The values of $\langle Z \rangle$ are observed to be in close agreement between MULTI-FS and PROPACEOS, which is expected since the same IPD model is employed by these two codes. Compared to MULTI-FS, a relatively lower $\langle Z \rangle$ is predicted from FLYCHK with the mEK model when the temperature is below 20 eV and a higher $\langle Z \rangle$ above 20 eV, exceeding the MULTI-FS $\langle Z \rangle$ by 0.65 at 40 eV. For FLYCHK with the SP model, a similar behavior is observed, but with the crossover point at around 30 eV compared to MULTI-FS. Importantly, within a target temperature range of 20 ± 2 eV at the two time delays of interest as shown in Fig. 1(d), FLYCHK with the mEK prescription of IPD and PROPACEOS both give an average ionization reasonably close to that with MULTI-FS, ensuring the consistency of $\langle Z \rangle$ for the hydro simulation data in this range.

It is possible that, due to the delayed heating of the ion lattice, the actual onset of expansion lags the prediction from the hydro simulations. Thus, as a limiting case, we also make comparisons to an isochoric slab model which assumes no hydrodynamic expansion, as shown in Figs. 3(c) and 3(d). A hydrodynamic simulation with MULTI-FS code was carried out in which the hydrodynamic motion was turned off. The electron-ion coupling was left on in the simulation and was based on the Drude-Sommerfeld model, as employed in the previous simulations. The resultant electron temperature profiles at the two time delays of interest show a temperature range from 21 to 25 eV, which is higher than the previous cases with hydrodynamic motion. For these calculations, the three IPD models were employed. It appears that the measurements agree better with the simulation results obtained with the mEK model at $t = 0.5$ ps. At $t = 1.0$ ps all the predictions agree within the error bars. For the Al^{5+} absorption line, the calculations without hydrodynamic expansion indicate better agreement in absorption depth with the measurements than the calculations based on the full MULTI-FS hydrodynamic simulation, indicating that the detailed hydrodynamic behavior may be important early in the interaction.

V. CONCLUSION

In conclusion, the first experiment using betatron radiation to probe warm dense aluminum via K-shell line absorption spectroscopy has been demonstrated as an alternative means to study this difficult-to-measure regime of material science. Warm dense aluminum was produced by irradiating a free-standing nanofoil with a femtosecond optical laser pulse and was heated to an electron temperature of ~20–25 eV with a near-solid mass density. Absorption dips in the transmitted x-ray spectrum produced by the Al^{4+} and Al^{5+} ions were clearly seen in the experiments. The measured absorption spectra were compared to simulations with various IPD models, including the commonly used SP model and an alternative mEK model. Disagreement between measurement and simulation at the Al^{5+} position was observed. While the error bar in the present measurement is large, this perhaps suggests that the nonequal electron and ion temperatures and slower than predicted onset of hydrodynamic expansion might be important early in the interaction. However, further measurements with an improved accuracy and improved signal-to-noise ratio are required to allow more accurate comparisons with the models.

ACKNOWLEDGMENTS

The authors would like to thank the technical staff at the Advanced Laser Light Source facility for their expert assistance throughout the experiments. The authors would also like to thank Prof. T. Ozaki from INRS for his help and his participation in the development of the betatron beam line and in its use and to thank Sam Vinko of the University of Oxford for helpful discussions. This work was funded by the Natural Sciences and Engineering Research Council of Canada Grant No. 2014-05736, the Canadian Foundation for Innovation, and the Fonds de recherche du Québec—Nature et technologies.

[1] M. Ross, Nature **292**, 435 (1981).
[2] L. R. Benedetti *et al.*, Science **286**, 100 (1999).
[3] Z. Chen *et al.*, Phys. Rev. Lett. **108**, 165001 (2012).
[4] S. M. Vinko *et al.*, Nature **482**, 59 (2012).
[5] O. Ciricosta *et al.*, Phys. Rev. Lett. **109**, 065002 (2012).
[6] A. Mančić *et al.*, Phys. Rev. Lett. **104**, 035002 (2010).

[7] P. B. Corkum *et al.*, Phys. Rev. Lett. **61**, 2886 (1988).
[8] Z. Lin *et al.*, Phys. Rev. B **77**, 075133 (2008).
[9] G. Ecker and W. Kröll, Phys. Fluids **6**, 62 (1963).
[10] J. C. Stewart and K. D. Pyatt Jr., Astrophys. J. **144**, 1203 (1966).
[11] G. Zimmerman and R. More, J. Quant. Spectrosc. Radiat. Transfer **23**, 517 (1980).
[12] R. M. More, Adv. At. Mol. Phys. **21**, 305 (1985).
[13] D. J. Hoarty *et al.*, Phys. Rev. Lett. **110**, 265003 (2013).
[14] L. B. Fletcher *et al.*, Phys. Rev. Lett. **112**, 145004 (2014).
[15] A. Forsman *et al.*, Phys. Rev. E **58**, R1248(R) (1998).
[16] F. Albert *et al.*, Phys. Rev. E **77**, 056402 (2008).
[17] T. P. Kim *et al.*, Phys. Rev. Lett. **97**, 225002 (2006).
[18] S. Fourmaux *et al.*, Opt. Lett. **36**, 2426 (2011).
[19] M. Z. Mo *et al.*, Rev. Sci. Instrum. **84**, 123106 (2013).
[20] https://www.nist.gov/pml/atomic-spectra-database
[21] T. R. Preston *et al.*, High Energy Density Phys. **9**, 258 (2013).
[22] R. M. More, in *Applied Atomic Collision Physics, 2* (Academic Press, New York, 1982).
[23] S. Fourmaux *et al.*, Opt. Express **16**, 11987 (2008).
[24] S. Fourmaux *et al.*, Opt. Express **19**, 8486 (2011).
[25] T. E. Hartman, J. Vac. Sci. Technol. **2**, 239 (1965).
[26] R. Ramis *et al.*, Comput. Phys. Commun. **183**, 637 (2012).
[27] K. Eidmann *et al.*, Phys. Rev. E **62**, 1202 (2000).
[28] A. Tronnier, Absorption von VUV-Photonen in Warm Dense Matter, Ph.D. thesis, Technical University Munich, 2007.
[29] A. J. Kemp and J. Meyer-ter Vehn, Nucl. Instrum. Methods Phys. Res. Sec. A **415**, 674 (1998).
[30] K. Eidmann, Laser Part. Beams **12**, 223 (1994).
[31] J. J. Macfarlane *et al.*, in Proceedings of Inertial Fusion and Science Applications, La Grange Park, IL (2003).
[32] http://nlte.nist.gov/FLY/
[33] H.-K. Chung *et al.*, High Energy Density Phys. **3**, 57 (2007).
[34] S. M. Vinko *et al.*, Nature Commun. **5**, 3533 (2014).
[35] http://www.prism-cs.com/Software/PROPACEOS/PROPACEOS.htm